Investigation of Dy^{3+} Ion Doped Borate Glasses and Their Potential for WLED and Laser Application

Juniastel Rajagukguk[1*], Lia Yuliantini[2], Fitrilawati[3], Mitra Djamal[2,4] & Jakrapong Kaewkhao[5,6]

[1]Department of Physics, Faculty of Mathematics and Natural Sciences, Universitas Negeri Medan, 20221, Indonesia
[2]Department of Physics, Faculty of Mathematics and Natural Sciences, Institut Teknologi Bandung, Jalan Ganesa No. 10, Bandung 40132, Indonesia
[3]Department of Physics, Faculty of Mathematics and Natural Science, Universitas Padjadjaran, Sumedang 45363, Indonesia
[4]Physics Study Program, Department of Science, Institut Teknologi Sumatera, Lampung 35365, Indonesia
[5]Center of Excellence in Glass Technology and Materials Science (CEGM), Nakhon Pathom Rajabhat University, Nakhon Pathom 73000, Thailand
[6]Physics Program, Faculty of Science and Technology, Nakhon Pathom Rajabhat University, Nakhon Pathom 73000, Thailand
*E-mail: juniastel@unimed.ac.id

Highlights:

- Glass with formula $(65\text{-}x)B_2O_3{:}15Na_2O{:}10PbO{:}5ZnO{:}5Li_2O{:}xDy_2O_3$ (x = 0.0; 0.05; 0.1; 0.5; 1.0; 2.0 mol%) was developed using the melt and quenching technique.
- The range of direct and indirect bandgap value for all samples was 2.84 to 3.57 eV.
- The strongest absorption band was found at a wavelength of 1270 nm ($^6H_{15/2} \rightarrow {}^6H_{9/2} + {}^6F_{11/2}$).
- The emission spectra and CIE 1931 chromaticity confirmed the white emission of the glasses when excited by 349 nm.
- The JO parameter of the glasses was $\Omega_2 > \Omega_6 > \Omega_4$ with a high lasing parameter.

Abstract. In this research, Dy^{3+} ion-doped Na_2O-PbO-ZnO-Li_2O-B_2O_3 glasses were developed using the melt and quenching method. The addition of Dy^{3+} ions in the glass improved the optical properties. The XRD graph verified the amorphous of the glass sample. FTIR showed the vibration of BO_3 and BO_4 in the structure of the glass. The enhancement of NBOs in the structure of the glass affected the reduction of the bandgap energy of the glass. The hypersensitive transition of the present glass was found at 1270 nm (infrared region) due to electron movement from the $^6H_{15/2}$ level to the $^6H_{9/2}$+$^6F_{11/2}$ level. The strong white emission of the glasses came from 575 nm (yellow region) and 483 nm (blue region) when excited by 349 nm. The CIE 1931 chromaticity was located at (0.37;0.40) and verified the white emission of the glasses. Meanwhile, the trendline of the JO parameter was $\Omega_2 > \Omega_6 > \Omega_4$, indicating the high ionic character of the glass structure. The value of the calculated branching ratio and emission cross-section of Dy_1.0 glass was 0.64 and 0.90 x 10^{-20} cm^2, respectively. From

Received December 10th, 2019, Revised April 13th, 2020, Accepted for publication September 17th, 2020.
 ISSN: 2337-5779,
DOI: 10.5614/j.eng.technol.sci.2020.52.6.9

the analysis of results, the present glass has high potential for WLED and laser application.

Keywords: *borate glass; laser; luminescence; trivalent dysprosium; WLED.*

1 Introduction

Photonics devices such as lasers, solid-state lighting and thermoluminescence sensors are widely used in our daily life. The optical gain medium is an important part of an illumination source. Solid-state lighting commonly uses semiconductors, organic or polymer materials as illumination source. The most popular optical gain is composed of a crystal material as the host matrix. However, the downside of crystal materials is that their development highly complex and production is high cost. Glass is a potential material to replace crystal as the host matrix. Glass has extraordinary characteristic, such as high transparency and a high refractive index. Moreover, the development of glass is simple and production is low-cost. Trivalent rare-earth ions including Dy^{3+}, Sm^{3+}, Pm^{3+}, Eu^{3+} and Er^{3+}, which can act as dopant in glass systems such as borate, silicate, phosphate, and tellurite [1].

They produce intensely visible to infrared emissions due to f-f transition. Among glass types, borate glass has interesting behavior because of the modification of BO_3 to BO_4 with the addition of oxide glass. Borate glass has a lower melting point than silicate glass, high transparency and good thermal stability. In the Eu^{3+} ion case, the reduction of the B_2O_3 glass concentration can increase the luminescence intensity [2]. In another case, the addition of B_2O_3 decreases the BO_4 unit and increases the number of BO_3 units indicating that most of the BO_4 units are converted to BO_3 units [3]. The addition of R_2O such as Na, Li or K improves the glass structure, including BO_4 or NBO formation. The addition of Na_2O in the glass host can reduce the glass bonding strength and decrease the probability of spontaneous emission [4,5]. It is well known that borate has high phonon energy, around 1500 cm^{-1}, the addition of PbO in borate glass can reduce the phonon energy due to the higher molecular weight [6]. The addition of ZnO in the glass host can increase the glass-forming ability and the refractive index [7]. Meanwhile, a mix of Li_2O can produce a bubble-free and highly stable glass [8].

The addition of Dy^{3+} in glasses such as tellurium-borate glass [9], tellurite glasses [10], borotellurite glasses [11], silicate glass [12], fluorosilicate glass [13] and borosilicate glasses [14] has been investigated. It was shown that Dy^{3+} ion-doped glasses generated a strong white emission, which makes them suitable for solid-state lighting (SSL) or white illumination applications. The white emission of

Dy^{3+} ions was generated from the combination of yellow and blue light under ultraviolet excitation.

A variety of glass compositions can improve the ratio of yellow and blue emission (Y/B). From previous work, yellow and blue emission, respectively, originate from a $^4F_{9/2} \rightarrow {}^6H_{13/2}$ (~570 nm) transition and $^4F_{9/2} \rightarrow {}^6H_{15/2}$ (~480 nm) transition. The Y/B ratio can be adjusted by the host material, the Dy^{3+} ion concentration and the excitation wavelenght [10]. The proper material combination is a crucial problem to be solved to find better properties, such as a long lifetime and high emission intensity.

We found that Dy^{3+} ion doped Na_2O-PbO-ZnO-Li_2O-B_2O_3 glass has not been investigated. Therefore, in this research, we investigated the structural, optical, photoluminescence and radiative properties of this glass to understanding their future application, especially for WLED and laser applications. The Judd-Ofelt (JO) theory was used to predict the glasses' lasing potential parameters, including the Judd-Ofelt (JO) parameter ($\Omega_{\lambda = 2,4,6}$), the oscillator strength (*f*), the radiative transition probability (A_R), the stimulated emission cross-section (σ_e) and the branching ratio (β_R).

2 Method

2.1 Glass Preparation and Characterization

In this research, the glasses were manufactured using a conventional method, namely melt and quenching. The glass molar composition was (65-x)B_2O_3:15Na_2O:10PbO:5Li_2O:5ZnO:xDy_2O_3 (x = 0.0; 0.05; 0.1; 0.5; 1.0; 2.0 mol%). The glass samples were labeled as Dy_0.0, Dy_0.05, Dy_0.1, Dy_0.5, Dy_1.0 and Dy_2.0, respectively. Twenty grams of raw material with high purity (95-99 %) from Sigma Aldrich was used. The batch material was kept in tanhe alumina crucible and melted in an electric furnace at 1200 °C for 4 hours. Afterwards, the glassy mass was poured out immediately on a preheated stainless steel plate. For releasing the residual stresses, the glass samples were annealed at 300 °C for 3 hours.

For the measurement of their properties, the glass samples were cut into a shape of 10 x 10 x 3 mm^3 and then polished. X-ray powder diffraction (XRD) and Fourier-transform infrared spectroscopy (FTIR) were used to study the glass structure while the refractive index and absorption spectra were measured to investigate the optical properties. A UV-VIS-NIR spectrophotometer (Shimadzu 3600) was used to obtain the optical absorption spectrum of the glass samples. The photoluminescence properties were observed using a fluorescence spectrophotometer (Cary Eclipse) produced by Agilent Technology Inc.

The physical properties were obtained by weighing the glass samples following Archimedes' law [12]. Radiative properties, including JO parameter (Ω_λ); experiment (f_{exp}) and calculated oscillator strength (f_{cal}); stimulated emission cross-section (σ_e); radiative transition probability (A_R); experiment (β_{exp}) and calculated branching ratio (β_{cal}); and radiative lifetime (τ_{rad}), were analyzed using FORTRAN, where Judd Ofelt theory [15,16] was implemented in the program. The program has been used in previous works such as [11-13].

3 Results and Discussion

3.1 Physical and Structural Properties

Figure 1 shows the density and molar volume of the glasses. The glass samples' density increased with the presence of Dy_2O_3 concentration from 0.1 to 2 mol% due to the larger molecular mass of Dy_2O_3 compared to B_2O_3. The density of Dy_1.0 glass is 2.98 gcm^{-3}, which is higher than that of S6 glass [14] and Dy_2O_3 doped lithium borate glass [17]. The enhancement of molar volume occurs with the increase of the Dy_2O_3 concentration, indicating excessive NBOs in the glass structure. The NBO units influence BO_3 or BO_4 formation in the glass structure following the reaction $BO_3 + NBO \rightarrow BO_4$.

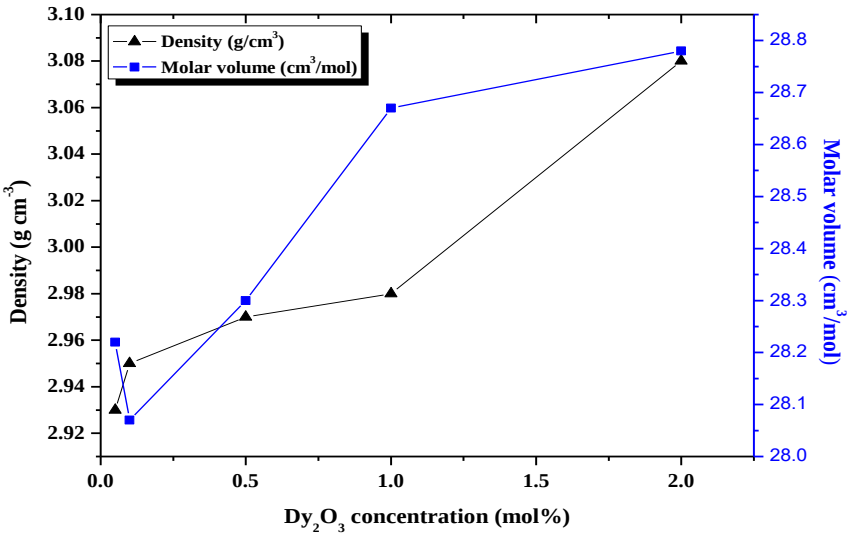

Figure 1 Density and molar volume graph of Dy^{3+} ion-doped Na_2O-PbO-ZnO-Li_2O-B_2O_3 glasses.

The merging of NBO units contributes to the enrichment of the BO_4 units in the structure of the glass [3]. Figure 2(a) reveals the FTIR spectra of the Dy^{3+} ion-

doped Na_2O-PbO-ZnO-Li_2O-B_2O_3 glasses, offering 5 bands from 680 to 4000 cm^{-1}. The FTIR band centered at 680 cm^{-1} confirms the bending mode vibrations of B-O-B linkage [18].

The FTIR band of 844 cm^{-1} is raised because of the asymmetric stretching mode of B-O units in BO_4 [19]. The strong band at 1189 cm^{-1} shows up because of B–O bond stretching vibration mode with NBO atoms in the symmetric BO_3 units and asymmetric stretching vibration mode of B-O bonds in the [BO_4] unit from ortho-borate and pyro-borate groups [20,21]. Water, B-OH hydroxyl and OH group vibrations emerge at 2924 cm^{-1} and 3387 cm^{-1} [18].

The list of wavenumbers and the assignment of FTIR is presented in Table 1. Figure 2(b) presents the XRD pattern of the glass samples with various Dy^{3+} contents from 0.0 mol% to 2.0 mol%. All samples of Dy_2O_3 doped Na_2O-PbO-ZnO-Li_2O-B_2O_3 glasses, including the undoped (Dy_0.0) sample, exhibited an amorphous nature with a broad hump at around 20 to 30 degrees.

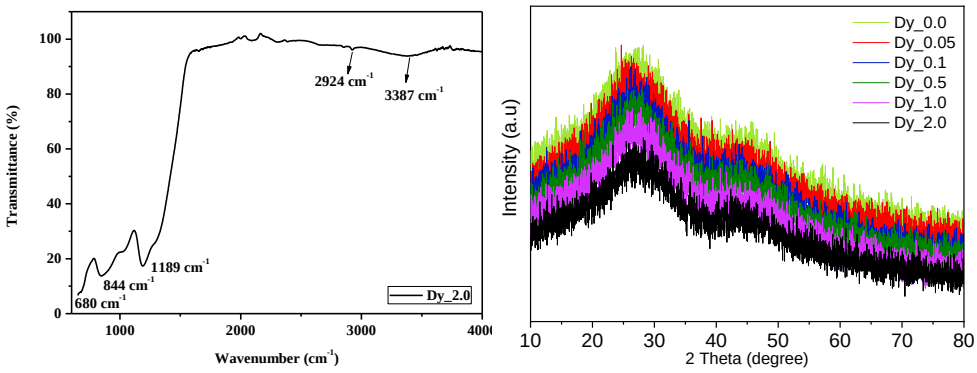

(a) (b)

Figure 2 (a) FTIR spectra and (b) XRD pattern of 2 mol Dy_2O_3 doped Na_2O-Li_2O-ZnO- B_2O_3 glasses.

Table 1 Wavenumber and assignment of FTIR spectra of trivalent dysprosium ion-doped Na_2O- Li_2O-ZnO- B_2O_3 glasses.

Wavenumber (cm^{-1})	Assignment	Ref
680	B-O-B bending mode vibrations	[18]
844	Asymmetric stretching mode of B–O unit in BO_4	[19]
1189	B–O bond stretching vibration in symmetric BO_3 units with bridging oxygen atoms, B-O bonds asymmetric stretching mode vibrations in [BO_4] units from ortho-borate and pyro-borate groups	[20,21]
2924, 3387	Water, B-OH hydroxyl and OH groups vibrations	[18]

3.2 Optical Properties

The optical band gap shows the threshold value of photons to be absorbed. It is well known that glass has an amorphous and disorderly structure. The absorption edge will be shifted due to the modification of oxygen binding that influences NBO formation.

Electrons in ground state will move to excited state when the photons of the initial light are absorbed by the material, and the electron transition can be direct or indirect [22]. From the optical band gap, the electronic structure of the material can be understood. Figure 3(a) and (b) show the direct and indirect bandgap of Dy_00 to Dy_2.00 glass. The absorption spectra of the glasses were extracted to obtain the optical band gap following Eq. (1).

$$\alpha = \frac{\alpha_0 \left(h\nu - E_g^{opt}\right)^n}{h\nu} \tag{1}$$

where α is the coefficient of absorption, and E_g^{opt} is the optical bandgap. Meanwhile, 'n' shows the typical optical transition and Tauc's plot obliges n = ½ for direct and n = 2 for indirect transition [12]. For the oxide glass system, Eq. (1) can be written as $(\alpha h\nu)^{1/2} = \alpha_0 \left(h\nu - E_g^{opt}\right)^n$.

The values of the optical band gap were analyzed by plotting $(\alpha h\nu)^{1/2}$ as a function of $h\nu$. E_{opt} was obtained by linear extrapolation of the x-intercept fitted to high $h\nu$ data. Plots of $(\alpha h\nu)^2$ versus $h\nu$ and $(\alpha h\nu)^{1/2}$ versus $h\nu$ for direct and indirect transitions respectively are shown in Figure 3. The direct and indirect bandgap of Dy^{3+} ion-doped glasses were 2.84 to 3.57 eV, as shown in Table 2. The direct and indirect bandgap decreased with the addition of Dy_2O_3 concentration in the structure of glass.

The presence of Dy^{3+} ions in the glass structure effects the conversion of BO_3 units to BO_4 unit and increases NBO formation. They donate more electrons and move the electronic state closer to the conduction band. This induces the reduction of the bandgap energy [23,24]. The ionic structure of the NBOs causes high polarizability of material so that the present glass has a high tendency to polarize [25]. Figure 4 presents the trend line of the direct and indirect bandgap of the present glass.

The absorption spectra were studied between a wavelength of 320 nm to 1850 nm as presented in Figure 5. Several absorption bands, i.e. 349 nm, 363 nm, 387 nm, 426 nm, 452 nm, 473 nm, 754 nm, 801 nm, 900 nm, 1090 nm, 1270 nm and 1680 nm, occur due to electron transition from $^6H_{15/2}$ level.

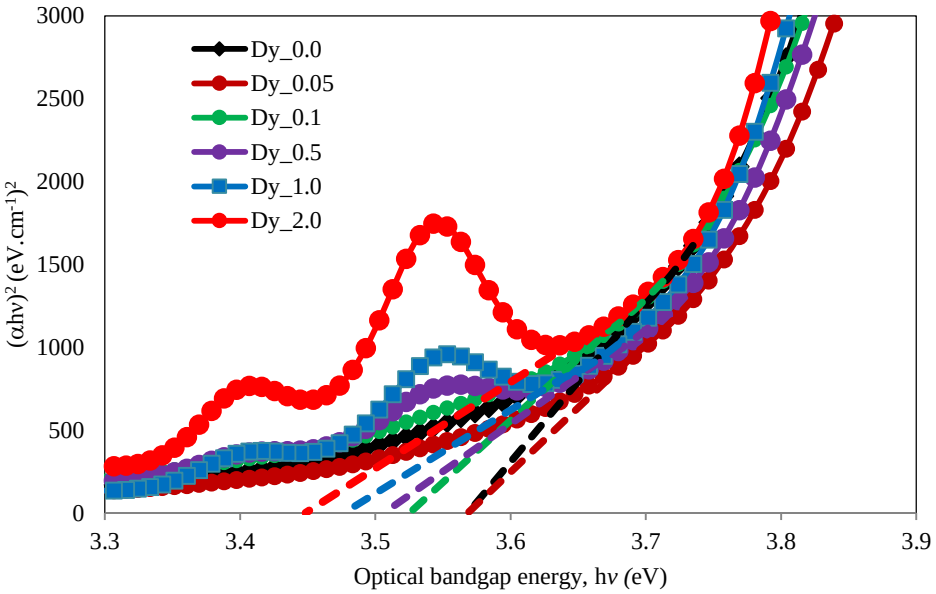

(a)

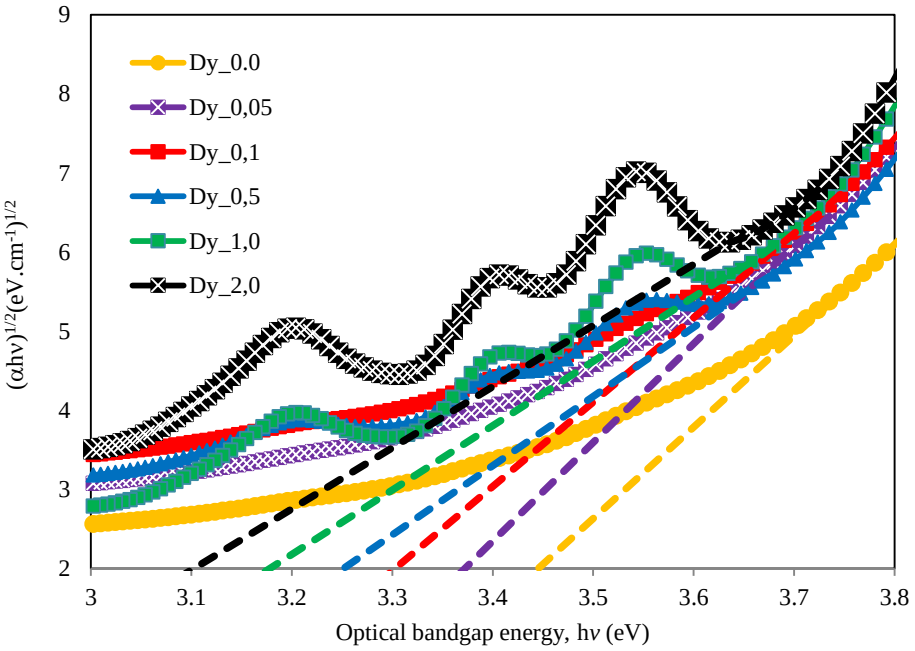

(b)

Figure 3 (a) Direct bandgap energy and (b) indirect bandgap energy of Dy^{3+} doped glasses.

Table 2 Direct and indirect bandgap energy of Dy^{3+} doped glasses.

Glasses	Dy_0.0	Dy_0.05	Dy_0.1	Dy_0.5	Dy_1.0	Dy_2.0
Direct E_g	3.57	3.57	3.53	3.51	3.48	3.45
Indirect E_g	3.27	3.21	3.12	3.02	2.93	2.84

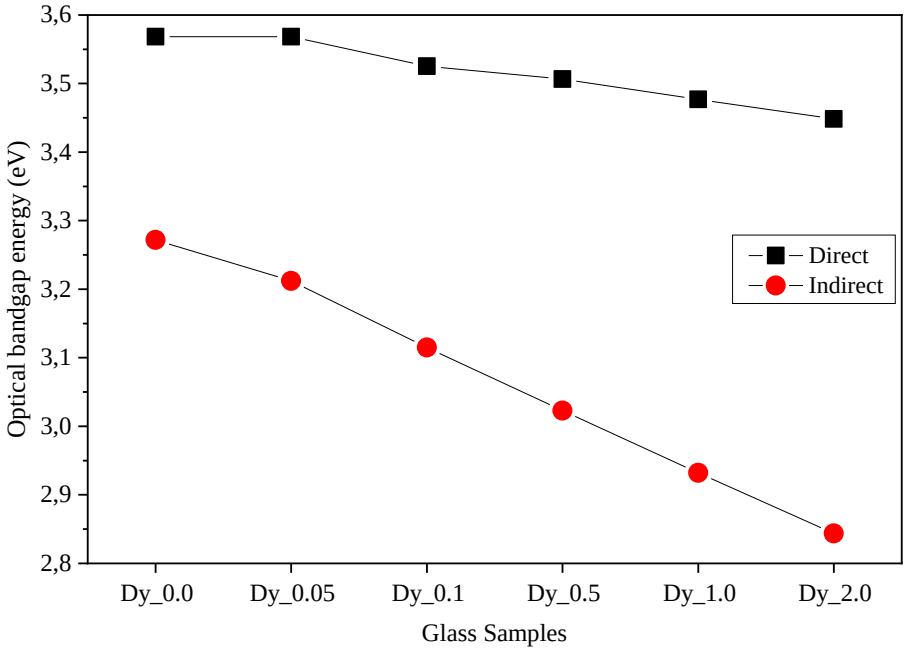

Figure 4 Distribution of direct and indirect bandgap energy of Dy^{3+} ions in the glass system.

The absorption bands correspond with excited states such as $^6P_{3/2}$, $^6P_{5/2}$, $^4I_{13/2}$+$^4F_{7/2}$, $^4G_{11/2}$, $^4I_{15/2}$, $^4F_{9/2}$, $^6F_{3/2}$, $^6F_{5/2}$, $^6F_{7/2}$, $^6H_{7/2}$+$^6F_{9/2}$, $^6H_{9/2}$+$^6F_{11/2}$ and $^6H_{11/2}$ level, respectively. The excited levels are comparable with reported data [26-28].

The absorption intensity increased with enhancement of the Dy_2O_3 concentration in the glass structure. The alteration of Dy^{3+} ions in the glass system slightly shifts the absorption band, as shown in Table 3. The sharpest absorption bands, emerging at 1270 nm in the infrared region, are generated from the $^6H_{15/2}$ level to the $^6H_{9/2}$+$^6F_{11/2}$ level.

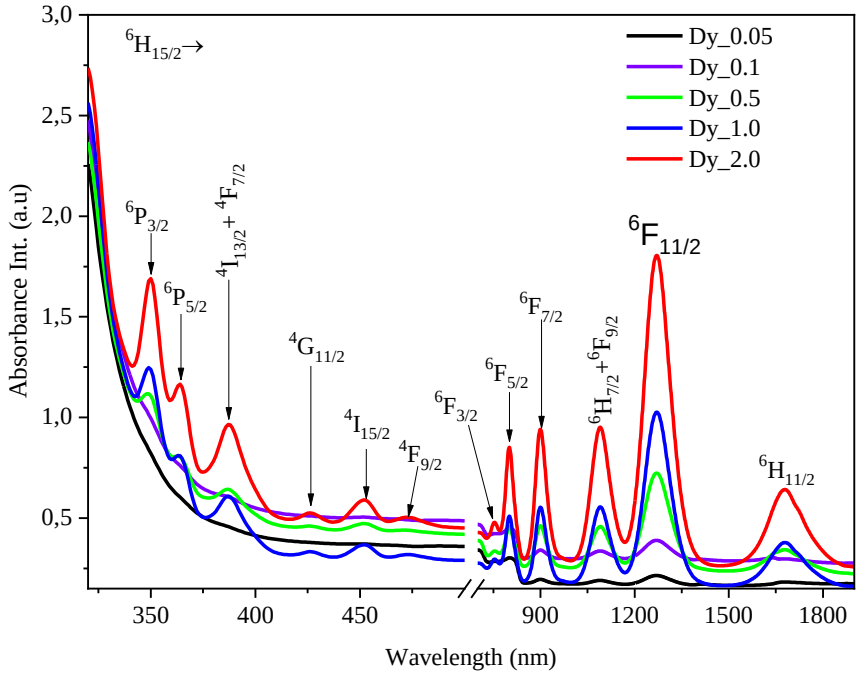

Figure 5 Optical absorption spectra of Dy^{3+} doped glasses.

Table 3 Experimental oscillator strength (fexp) and calculated oscillator strength (fcal) values (x 10-6) of trivalent dysprosium ion in the glass systems.

Transitions $^6H_{15/2}\rightarrow$	Dy_0.5			Dy_1.0			Dy_2.0		
	λ_{abs} (nm)	f_{exp}	f_{cal}	λ_{abs} (nm)	f_{exp}	f_{cal}	λ_{abs} (nm)	f_{exp}	f_{cal}
$^6P_{3/2}$	348	3.18	2.68	349	3.73	2.86	350	3.65	2.68
$^6P_{5/2}$	363	1.34	1.64	363	1.95	1.75	364	1.00	1.64
$^4F_{7/2}+^4I_{13/2}$	387	2.63	2.86	387	3.50	3.03	387	2.60	2.62
$^4G_{11/2}$	426	0.49	0.25	426	0.36	0.26	426	0.37	0.21
$^4I_{15/2}$	452	0.88	1.55	452	1.61	1.65	452	0.90	1.56
$^4F_{9/2}$	471	0.40	0.60	473	0.85	0.64	473	0.50	0.59
$^6F_{3/2}$	754	0.79	0.69	754	1.16	0.74	753	0.49	0.69
$^6F_{5/2}$	800	5.53	3.68	801	5.42	3.93	801	4.22	3.69
$^6F_{7/2}$	900	7.38	7.76	900	8.36	8.29	900	7.89	7.63
$^6H_{7/2}+^6F_{9/2}$	1090	9.45	9.40	1090	9.92	10.01	1090	8.79	8.87
$^6H_{9/2}+^6F_{11/2}$	1270	21.59	21.55	1270	22.57	22.52	1271	20.85	20.82
$^6H_{11/2}$	1678	4.18	4.47	1680	4.31	4.75	1679	4.23	4.46
RMS deviation	± 0.621			±0.554			±0.436		

3.3 Luminescence Properties

Figure 6(a) reveals the excitation spectra that were measured between the wavelength of 300 nm to 550 nm with λ_{em} = 575 nm. The electrons from the $^6H_{15/2}$ level were excited to $^6P_{3/2}$, $^6P_{7/2}$, $^6P_{5/2}$, $^4I_{13/2}$+$^4F_{7/2}$, $^4G_{11/2}$, $^4I_{15/2}$ and $^4F_{9/2}$ level, comparable with previous work [26,29]. The highest peak of the excitation spectra came from the $^6H_{15/2} \rightarrow {}^6P_{7/2}$ transition centered at 349 nm. Figure 6(b) displays the emission spectra that were observed between 420 nm to 800 nm and 349 nm as excitation wavelength (λ_{ex}).

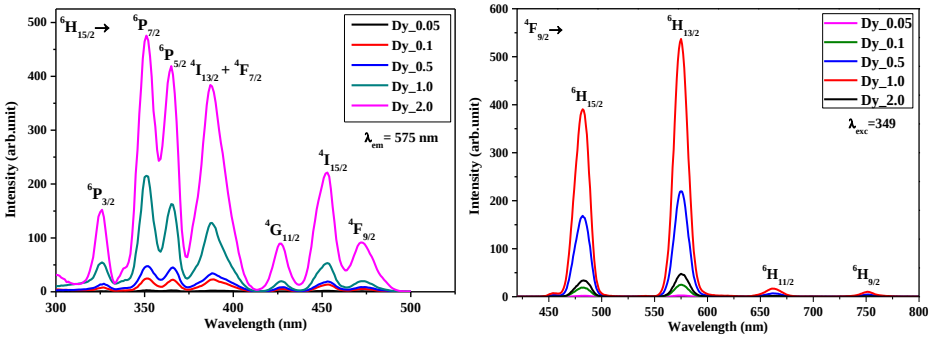

Figure 6 (a) Excitation spectra with λem = 575 nm, and (b) emission spectra of Dy^{3+} doped Na_2O-PbO-ZnO-Li_2O-B2O_3 glasses with λex = 349 nm.

The emission intensity became more intense with the addition of Dy_2O_3 at a concentration of 0.05 mol% to 1.0 mol% due to the increasing absorption intensity from the pump source at the initial concentration. However, the emission intensity decreased with the addition of Dy_2O_3 concentration to 2.0 mol%. A reduction of the emission intensity due to absorption saturation was achieved in this stage and the emission intensity rate began to decrease [30]. This is well known as a quenching effect between Dy^{3+} ions, where the clustering of ions speedily shortens the distance between Dy^{3+} ions. Therefore, the optimal concentration of Dy^{3+} ions was found in the Dy_1.0 specimen. When the glass sample was excited, the metastable $^4F_{9/2}$ level was generated and electrons from the excited level immediately fell to the $^4F_{9/2}$ level. This is a non-radiative transition, where phonons are generated as released energy. Afterwards, the electrons from the metastable $^4F_{9/2}$ level go down to the $^6H_{15/2}$ (483) nm, $^6H_{13/2}$ (575) nm, $^6H_{11/2}$ (665) nm and $^6H_{9/2}$ (753) nm level, comparable with [9,12].

In the emission spectra, the highest emission peak came from the $^4F_{9/2} \rightarrow {}^6H_{13/2}$ transition centered at 575 nm (yellow region). This occurs because the collusion strength calculation shows that, in the same energy range, excitation from ground

level to $^6H_{13/2}$ level was higher than at $^6H_{11/2}$ and $^6H_{9/2}$ level. Therefore, it predicts that the$^6H_{13/2}$ level is more populated than the other levels in electron collusion excitation [28]. The second sharp light emission is centered at 483 nm (blue region) due to $^4F_{9/2} \rightarrow {}^6H_{15/2}$ transition. The blue region is generated by the magnetic-dipole mechanism while the yellow region is affected by the electronic-dipole mechanism. The combination of yellow and blue emission of Dy^{3+} ions in the glass system contributes to white emission, as shown Figure 7(b).

3.4 Radiative Properties

The experimental and calculated oscillator strengths of Dy_0.5, Dy_1.0, and Dy_2.0 are presented in Table 3. The highest oscillator strength was obtained from the strongest absorption band centered at 1271 nm due to $^6H_{15/2} \rightarrow {}^6H_{9/2} + {}^6F_{11/2}$ transition. The strongest absorption spectra transition is known as the hypersensitive transition. This transition respects the selection rule following $|\Delta S|=0$, $|\Delta L|\leq 2$ and $|\Delta J|\leq 2$ [27]. Table 4 shows the Judd-Ofelt (JO) parameters (Ω_λ), effective bandwidth ($\Delta\lambda_{eff}$), branching ratio (β_R), stimulated emission cross-section (σ_e), radiative lifetime (τ_R) and radiative transition probability (A_R) of the present glass and the reported Dy^{3+}: glasses for the $^4F_{9/2} \rightarrow {}^6H_{13/2}$ transition.

Table 4 Judd-Ofelt parameters (Ωλx10-20 cm2), effective bandwidth (Δλeff, nm), emission cross-section (σe x 10-20 ,cm2), branching ratio (βR,%), radiative transition probability (AR, s-1) and color coordinate (x,y) of present glass and reported Dy3+: glassess for the 4F9/2→6H13/2 transition (λp = 575 nm).

Glass	Ω_2	Ω_4	Ω_6	Trendline	$\Delta\lambda_{eff}$	σ_e	β_R	A_R	(x,y)
Dy_0.5 [p.w]	19.85	6.66	8.64	$\Omega_2>\Omega_6>\Omega_4$	15.94	0.81	0.64	2430	0.36,0.41
Dy_1.0 [p.w]	20.76	7.08	9.33	$\Omega_2>\Omega_6>\Omega_4$	14.45	0.90	0.64	2446	0.37,0.40
Dy_2.0 [p.w]	20.68	5.82	9.03	$\Omega_2>\Omega_6>\Omega_4$	16.40	0.74	0.64	2293	0.36,0.40
TBZDy1.0 [11]	13.91	4.99	2.01	$\Omega_2>\Omega_4>\Omega_6$	10.25	0.07	0.78	510	0.42,0.43
TWLD1 [10]	5.895	0.93	1.22	$\Omega_2>\Omega_6>\Omega_4$	-	0.61	0.71	435	0.38,0.43
SKNPfLfDy1.0 [13]	10.02	4.84	2.70	$\Omega_2>\Omega_4>\Omega_6$	12.32	0.51	0.64	1194	-
A1 glass [29]	7.43	3.36	2.32	$\Omega_2>\Omega_4>\Omega_6$	-	0.15	0.63	507	0.40,0.43
LBGS-0.5Dy [12]	8.32	2.14	2.75	$\Omega_2>\Omega_6>\Omega_4$	18.93	0.48	-	878	0.41, 0.42
BGGD [30]	5.36	0.54	1.38	$\Omega_2>\Omega_6>\Omega_4$	-	-	-	-	-
ZNBBD-3 [32]	5.64	1.25	1.03	$\Omega_2>\Omega_4>\Omega_6$	13	0.24	0.61	609	-
LBZLFB [31]	14.44	5.23	5.71	$\Omega_2>\Omega_6>\Omega_4$	16	0.54	0.73	1478	0.29,0.34

The JO parameter of Dy_0.5, Dy_1.0 and Dy_2.0 glass was $\Omega_2 > \Omega_6 > \Omega_4$, which is similar to TWLD1 [10], LBGS-0.5Dy [12], BGGD [31] and LBZLFB [32]. The JO parameter of Ω_2 associated with the covalent and asymmetric nature of Dy^{3+} ions and the ligands of the glass structure. Meanwhile, the JO parameter of Ω_4 and Ω_6 shows the glass sample's viscosity and rigidity. The Ω_2 value of Dy_1.0 glass was the highest among the other glasses, indicating more asymmetry of the glass structure.The Dy_1.0 glass had larger σ_e than TBZDy1.0 [11], TWLD1

[10], SKNPfLfDy1.0 [13], A1 glass [29], LBGS-0.5Dy [12], ZNBBD-3 [33] and LBZLFB [32]. Among the other glass samples, the Dy_1.0 glass had high potential for high gain laser and low laser threshold application due to the highest σ_e and $\beta \geq 0.64$. It is well known that the requirement of β for laser application is ≥ 0.50. The radiative lifetime (τ_R) of the Dy_0.5, Dy_1.0 and Dy_2.0 glass was 0.283 ms; 0.260 ms; and 0.279 ms, respectively. Meanwhile, the total radiative transition probability of the Dy_0.5, Dy_1.0 and Dy_2.0 glass was 3531 s^{-1}, 3551 s^{-1} and 3312 s^{-1}, respectively.

3.5 Luminescence Decay Curve and CIE 1931 Chromaticity

Figure 7(a) is the decay curve of the Dy_0.05 to Dy_2.0 glass samples for $^4F_{9/2} \rightarrow {}^6H_{13/2}$ transition excited by 349 nm. The experiment lifetime (τ_{exp}) is shown in the graph. The experimental lifetime was 0.787, 1.174, 1.348, 1.470, and 1.609 ms for Dy_0.05, Dy_0.1, Dy0.5, Dy_1.0 and Dy_2.0, respectively. Dy_1.0 had a longer experimental lifetime than 0.168 ms, 0.384 ms, 0.573 ms, and 0.370 ms corresponding to TWLD1 [10], TBZDy1.0 [11], LBGS-0.5Dy [12] and SKNPfLfDy1.0 glass [13], respectively.

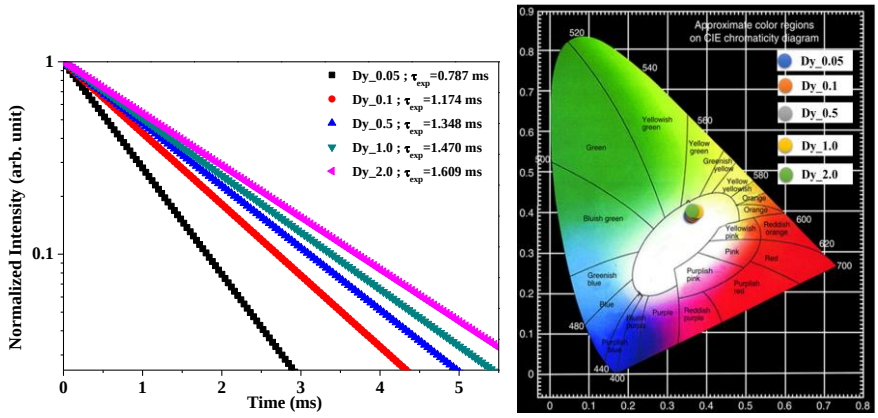

(a) (b)

Figure 7 (a) Decay time (lifetime), and (b) CIE 1931 chromaticity diagram for white emission of Dy^{3+} ion doped Na_2O-PbO-ZnO-Li_2O-B2O_3 glasses.

Color vision is a psychophysical phenomenon and color measurement should be determined where the results precisely correspond to human vision. Colorimetry is a way to accurately quantify and describe color vision, called the CIE 1931 chromaticity coordinate. Using the XYZ color matching function, the CIE 1931 chromaticity measures the color coordinate, called the tristimulus value [34].

Figure 7(b) shows the CIE 1931 chromaticity of all glasses with λ_{ex} = 349 nm. The color coordinate (x,y) of Dy_0.5, Dy_1.0, and Dy_2.0 was (0.36;0.41), (0.36;0.40), (0.36;0.41), (0.37;0.40) and (0.36;0.40), respectively. The addition of Dy_2O_3 in the glasses system did not significantly change the color coordinate of the glasses. They fell down to the white region, comparable to previous reports [9,35]. The strong white emission is due to the combination of yellow (575 nm transition from $^4F_{9/2}$ level to $^6H_{13/2}$ level) and blue (483 nm transition from $^4F_{9/2}$ level to $^6H_{15/2}$ level) emission. Therefore, the present glass is suitable for the optical gain medium of WLED applications [27].

4 Conclusion

We developed (65-x)B_2O_3:15Na_2O:10PbO:5Li2O:5ZnO:xDy_2O_3 (x = 0.0; 0.05; 0.1; 0.5; 1.0; 2.0 mol%) by using the melt and quenching technique. The glass sample density and molar volume have a tendency to increase by the addition of Dy_2O_3 concentration. Several bands were found from the FTIR spectra, including B-O-B linkage bending mode vibrations, B–O asymmetric stretching mode in BO_4, and hydroxyl (OH) group vibrations. The XRD graph confirmed the amorphousness of the sample with a broadening peak in the graph. The absorption spectra showed that the hypersensitive transition of all glass samples was centered at 1270 nm.

The emission spectra showed intense emission in the 483 nm (blue region) and 575 nm (yellow region). The color coordinate of the Dy_1.0 glass sample was (0.37,0.40), which is in the white region. The JO trend line of Dy_1.0 is $\Omega_2>\Omega_6>\Omega_4$. Since Dy_1.0 had a white emission coordinate with a high value of stimulated emission cross-section (σ_e= 0.90x10^{-20} cm^2) and branching ratios (0.64), it has high potential to be developed for WLED and laser applications.

Acknowledgments

The first author would like to thank Direktorat Riset dan Pengabdian Masyarakat (DRPM), Ministry of Research Technology and Higher Education and Universitas Negeri Medan for their financial support (Grant Number 076/SP2H/LT/DRPM/2019). One of the authors, Ms. Lia Yuliantini, would like to sincerely thank Prof. C.K. Jayasankar from Srivenkateswara University, India for her participation in the JO program.

References

[1] Varshneya, A.K., *Fundamentals of Inorganic Glasses*, Academic Press, Boston, 1994.

[2] Rajagukguk, J., Kaewkhao, J., Djamal, M., Hidayat, R. & Ruangtaweep, Y., *Structural and Optical Characteristics of Eu^{3+} Ions in Sodium-Lead-Zinc-Lithium-Borate Glass System*, J. Mole. Struct., **1121**, pp. 180-187. Oct. 2016.

[3] Jiao, Q., Li, G., Zhou, D. & Qiu, J., *Effect of the Glass Structure on Emission of Rare-Earth-Doped Borate Glasses*, J. Am. Ceram. Soc., **98**(12), pp. 4102-4106. Dec. 2015.

[4] Elbashar, Y.H., Rashad, M.M. & Rayan, D.A., *Physical and Mechanical Properties of Neodymium Doped Zinc Borate Glass with Different Boron Content*, Silicon., **10**(1), pp. 115-122, Jan. 2018.

[5] Rajagukguk, J., Sinaga, B. & Kaewkhao, J., *Structural and Spectroscopic Properties of Er^{3+} Doped Sodium Lithium Borate Glasses*, Spectrochimica Acta Part A: Molecular and Biomolecular Spectroscopy, **223**, 117342, Dec. 2019.

[6] Sołtys, M., Janek, J., Żur, L., Pisarska, J. & Pisarski, W.A., *Compositional-Dependent Europium-Doped Lead Phosphate Glasses and Their Spectroscopic Properties*, Optical Materials., **40**, pp. 91-96, Feb. 2015.

[7] Gayathri Pavani, P., Sadhana, K. & Chandra Mouli, V., *Optical, physical and Structural Studies of Boro-Zinc Tellurite Glasses*, Physica B: Condensed Matter, 406(6-7), pp. 1242-1247, Mar. 2011.

[8] Anjaiah, J., Laxmikanth, C., Veeraiah, N. & Kistaiah, P., *Infrared Luminescence and Thermoluminescence of Lithium Borate Glasses Doped with Sm3+ ions*, Materials Science-Poland. **33**(1), pp. 144-151, Mar. 2015.

[9] Li, B., Li, D., Pun, E.Y.B. & Lin, H., *Dy^{3+} Doped Tellurium-Borate Glass Phosphors for Laser-Driven White Illumination*, Journal of Luminescence, **206**(10), pp. 70-78, Feb. 2018.

[10] Kibrisli, O., Ersundu, A.E. & Ersundu, M.C., *Dy^{3+} Doped Tellurite Glasses for Solid-State Lighting: An Investigation Through Physical, Thermal, Structural and Optical Spectroscopy Studies*, Journal of Non-Crystalline Solids. **513**(3), pp. 125-136, Jun. 2019.

[11] Sandeep, K., Pandey, O.P., Jayasankar, C.K. & Chopra, N., *Spectroscopic, Thermal and Structural Investigations of Dy^{3+} Activated Zinc Borotellurite Glasses and Nano-Glass-Ceramics for White Light Generation*, Journal of Non-Crystalline Solids, **521**(5), 119472, Oct. 2019.

[12] Khan, I., Rooh, G., Rajaramakrishna, R., Srisittipokakun, N., Wongdeeying, C., Kiwsakunkran, N., Wantana, N., Kim, H.J., Kaewkhao, J. & Tuscharoen, S., *Photoluminescence and White Light Generation of Dy2O3 Doped Li2O-BaO-Gd2O3-SiO2 for White Light LED*, Journal of Alloys and Compounds, **774**(9), pp. 244-254, Feb. 2019.

[13] Manasa, P. &Jayasankar, C.K., *Spectroscopic Assessment of Dy3+ ions in Lead Fluorosilicate Glass as a Prospective Material for Solid State Yellow Laser*, Spectrochimica Acta Part A: Molecular and Biomolecular Spectroscopy, **212**(1), pp. 315-321, Apr. 2019.

[14] Kaur, R., Bhatia, V., Kumar, D., Rao, S.M.D., Singh, S.P. & Kumar, A., Physical, *Structural, Optical and Thermoluminescence Behavior of Dy_2O_3 Doped Sodium Magnesium Borosilicate Glasses*, Results in Physics, **12**, pp. 827-839, Mar. 2019.

[15] Judd, B.R., *Optical Absorption Intensities of Rare-Earth Ions*, Phys. Rev. **127**(3), pp. 750-761, Aug. 1962.

[16] Ofelt, G.S., *Intensities of Crystal Spectra of Rare-Earth Ions*, The Journal of Chemical Physics, **37**(3), pp. 511-520, Aug. 1962.

[17] Rimbach, A.C., Steudel, F., Ahrens, B. & Schweizer, S., *Tb3+, Eu3+, and Dy3+ Doped Lithium Borate and Lithium Aluminoborate Glass: Glass Properties and Photoluminescence Quantum Efficiency*, Journal of Non-Crystalline Solids, **499**, pp. 380-386, Nov. 2018.

[18] Hivrekar, M.M., Sable, D.B., Solunke, M.B. & Jadhav, K.M., *Network Structure Analysis of Modifier CdO Doped Sodium Borate Glass Using FTIR and Raman Spectroscopy*, Journal of Non-Crystalline Solids, **474**, pp. 58-65, Oct. 2017.

[19] Ozlem, Akgul, Nil Baran, Acarali, Nurcan, Tugrul, Emek Moroydor, Derun, Sabriye & Piskin, X-Ray, Thermal, FT-IR and Morphological Studies of Zinc Borate in Presence of Boric Acid Synthesized by Ulexite, Periodico Di Mineralogia, **83**(1), pp. 77-88, Apr. 2014.

[20] Doweidar, H., El-Egili, K., Ramadan, R. & Khalil, E., *Structural Species in Mixed-Fluoride PbF_2-CdF_2-B_2O_3 Borate Glasses; FTIR Investigation*, Vibrational Spectroscopy, **102**, pp. 24-30, Mei 2019.

[21] Thakur, S., Thakur, V., Kaur, A. & Singh, L., *Structural, Optical and Thermal Properties of Nickel Doped Bismuth Borate Glasses*, Journal of Non-Crystalline Solids, **512**, pp. 60-71, May 2019.

[22] Mohd Zaid, M.H., Matori, K.A., Abdul Aziz, S.Hj., Zakaria, A. & Mohd Ghazali, M.S., *Effect of ZnO on the Physical Properties and Optical Band Gap of Soda Lime Silicate Glass*, IJMS, **13**(6), pp. 7550-7558, Jun. 2012.

[23] El-Nahass, M.M., Soliman, H.S. & El-Denglawey, A., *Absorption Edge Shift, Optical Conductivity, and Energy Loss Function of Nano Thermal-Evaporated N-type Anatase TiO2 Films*, Appl. Phys. A., **122**(8), 775, Aug. 2016.

[24] Amjad, R.J., Sahar, M.R., Ghoshal, S.K., Dousti, M.R. & Arifin, R., Synthesis and Characterization of Dy^{3+} Doped Zinc-Lead-Phosphate Glass, Optical Materials, **35**(5), pp. 1103-1108, Mar. 2013.

[25] Halimah, M.K., Faznny, M.F., Azlan, M.N. & Sidek, H.A.A., *Optical Basicity and Electronic Polarizability of Zinc Borotellurite Glass Doped La3+ Ions*, Results in Physics, **7**, pp. 581-589, Jan. 2017.

[26] Carnall, W.T., Fields, P.R. & Rajnak, K., *Electronic Energy Levels in the Trivalent Lanthanide Aquo Ions. I. Pr^{3+}, Nd^{3+}, Pm^{3+}, Sm^{3+}, Dy^{3+}, Ho^{3+}, Er^{3+}, and Tm^{3+}*, The Journal of Chemical Physics, **49**(10), pp. 4424-4442, Nov. 1968.

[27] Deopa, N. & Rao, A.S., *Photoluminescence and Energy Transfer Studies of Dy^{3+} Ions Doped Lithium Lead Alumino Borate Glasses for w-LED and Laser Applications*, Journal of Luminescence, **192**, pp. 832-841, Dec. 2017.

[28] El-Maaref, A.A., Shaaban, K.H.S., Abdelawwad, M. & Saddeek, Y.B., *Optical Characterizations and Judd-Ofelt Analysis of Dy^{3+} Doped Borosilicate Glasses*, Optical Materials, **72**, pp. 169-176, Oct. 2017.

[29] Yuliantini, L., Kaewnuam, E., Hidayat, R., Djamal, M., Boonin, K., Yasaka, P., Wongdeeying, C., Kiwsakunkran, N. & Kaewkhao, J., *Yellow* and Blue Emission from BaO-(ZnO/ZnF2)-B_2O_3-TeO_2 Glasses Doped *with Dy^{3+} for Laser Medium and Scintillation Material Applications*, Optical Materials, **85**, pp. 382-390, Nov. 2018.

[30] Rajagukguk, J., Situmorang, R., Djamal, M., Rajaramakrishna, R., Kaewkhao, J. & Minh, P.H., *Structural, Spectroscopic and Optical Gain of Nd^{3+} Doped Fluorophosphate Glasses for Solid State Laser Application*, Journal of Luminescence, **216**, 116738. Dec. 2019

[31] Wang, W.C., Xiao, Y.B., Zhou, B., Xu, S.H. & Zhang, Q.Y., *Structural, Thermal, and Luminescent Properties of Germanate Glass Containing Heavily Dy_2O_3 Content*, Journal of Non-Crystalline Solids, **503-504**, pp. 400-408, Jan. 2019.

[32] Zulfiqar Ali Ahamed, Sd., Madhukar Reddy, C. & Deva Prasad Raju, B., *Structural, Thermal and Optical Investigations of Dy^{3+} Ions Doped Lead Containing Lithium Fluoroborate Glasses for Simulation of White Light*, Optical Materials, **35**(7), pp. 1385-1394, Mei 2013.

[33] Hegde, V., Chauhan, N., Viswanath, C.S.D., Kumar, V., Mahato, K.K. & Kamath, S.D., *Photoemission and Thermoluminescence Characteristics of Dy^{3+}-Doped Zinc Sodium Bismuth Borate Glasses*, Solid State Sciences, **89**, pp. 130-138, Mar. 2019.

[34] Dakin, J.P. & Brown, R.G.W., *Handbook of Optoelectronics*, CRC Press, 2010.

[35] Luewarasirikul, N., Kim, H.J., Meejitpaisan, P. & Kaewkhao, J., *White Light Emission of Dysprosium Doped Lanthanum Calcium Phosphate Oxide and Oxyfluoride Glasses*, Optical Materials, **66**, pp. 559-566, Apr. 2017.